OPEN ACCESS

University of BRISTOL

Nowacki, J., Mazlan, S. H., Osinga, H. M., & Tsaneva-Atanasova, K. T. (2009). The role of large-conductance Calcium-activated K+ (BK) channels in shaping bursting oscillations of a somatotroph cell model.

Early version, also known as pre-print

Link to publication record in Explore Bristol Research
PDF-document

University of Bristol - Explore Bristol Research
General rights

The role of large-conductance Calcium-activated K+ (BK) channels in shaping bursting oscillations of a somatotroph cell model

Jakub Nowacki,* Siti Mazlan,* Hinke M. Osinga,* Krasimira Tsaneva-Atanasova*

April 2, 2009

Abstract

We study a recently proposed somatotroph model that exhibits plateau bursting, a form of electrical activity that is typical for this cell type. We focus on the influence of the large conductance (BK-type) Ca^{2+}-activated K^+ current on the oscillations and duration of the active phase. The model involves two different time scales, but a standard bifurcation analysis of the fast-time limit does not completely explain the behavior of the model, which is subtly different from classical models for plateau bursting. In particular, the nullclines and velocities of the fast variables play an important role in shaping the bursting oscillations. We determine numerically how the fraction of open BK channels controls the amplitude of the fast oscillations during the active phase. Furthermore, we show how manifolds of the fast subsystem are involved in the termination of the active phase.

Keywords: Bursting, Nullclines, Stable manifolds, Fast-slow analysis

1 Introduction

Plateau bursting is a common pattern of electrical activity in hormone-secreting cells. Typical examples are the endocrine cells of the anterior pituitary gland, which are responsible for the secretion of hormones that, in turn, regulate a variety of other glands in the body [1, 2]. All of the anterior pituitary cells exhibit Ca^{2+}-dependent electrical activity that can vary significantly between cell types, ranging from spiking to bursting with distinct duration of the depolarized plateaus [1]. We focus on the behavior of a particular type of pituitary cell, namely, the somatotroph cell which releases growth hormone. Experimental data [1, 2, 3, 4] demonstrate that these cells fire plateau bursts of action potential (AP) associated with depolarization of the membrane potential (V_m). In turn, these plateau bursts induce Ca^{2+}-signals with an amplitude that is sufficient to trigger hormonal secretion [1, 2]. Clearly, a deeper insight into the mechanisms that

---

*Bristol Centre for Applied Nonlinear Mathematics, Department of Engineering Mathematics, University of Bristol, Queen's Building, University Walk, BS8 1TR

govern the generation and duration of bursts of AP and concurrent Ca^{2+} signals is an important step toward a better understanding of secretory responses.

In order to address these questions we study the somatotroph cell model introduced by Tsaneva-Atanasova et al. in [4]. This model is based on the classic Hodgkin-Huxley formalism [5, 6] and, therefore, incorporates the main biophysical determinants of the behavior of somatotrophs. Previous theoretical studies have focused on investigations of the effect of various currents on the electrical activity in pituitary somatotrophs [4] as well as phase resetting [7]. Here, we concentrate on the underlying dynamics of plateau bursting. Therefore, it suffices to study a simplified three-dimensional version of the model, which also allows for direct visualization of the bursting behavior. According to some bursting classifications [8], the model in [4] is an example of fold/subHopf bursting, also termed pseudo-plateau bursting [7]. Interestingly, compared with previously published models of fold/subHopf bursters [7, 9, 10, 11], our model is subtly different, because it features very small plateau oscillations. Moreover, its active phase ends rather abruptly in a way that appears to be unrelated to the underlying bifurcation structure of the fast subsystem.

The results in [4] suggest that the BK channels of the somatotroph cell play a key role in the initiation and the duration of plateau bursting. Modeling studies of other pituitary cell types have also shown that the magnitude of the BK current modulates the duration of plateau bursting [3, 10, 11]. Since BK channels are present in many cell types and influence a variety of cellular functions by controlling Ca^{2+}-influx [1, 2, 12], it is essential to explore their role in shaping the bursting oscillations.

In this paper we focus on the analysis of plateau-bursting oscillations in our model and the role of BK channels in the control of this phenomenon. In the next section we introduce a simplified version of the model in [4]. Section 3 presents a bifurcation analysis that is standard for fast-slow systems [13] and has been applied extensively in previous studies of fold/subHopf bursters [7, 9, 10, 11]. We demonstrate that the classical approach is unable to give a complete explanation of the dynamics found in our model. In section 4 we apply other dynamical systems techniques [14, 15], taking into account the effects of the nullclines and velocities of the fast variables on the frequency and amplitude of the oscillations during the active phase of a burst. In section 5 we address the question about the factors that determine the end of the active phase and the influence of the BK channels on its duration. All numerical computations were done using AUTO [16, 17] and XPP [18] and the visualizations were done in Matlab [19] with use of its Matplotlib tool.

2   The model

The model in this paper is a reduced version of the model presented in [4] and consists of three ordinary differential equations that describe the rates of change of the membrane potential V_m, the delayed-rectifier activation gating variable n_{dr} that governs the fraction of open K^+-channels, and the intracellular concentration $[Ca^{2+}]_i$ denoted by c. Here, we neglect the dynamics of the Ca^{2+} concentration in the endoplasmic reticulum and assume that it is constant at $Ca_{ER} = 167\mu M$; namely, during plateau bursting in the full model $[Ca^{2+}]_{ER}$ oscillates with very small amplitude

around an average value of about 167μM [4]. Hence, this is a reasonable assumption that allows for a dimension reduction. The simplified equations are as follows:

$$\frac{dV_m}{dt} = -\frac{1}{C_{\mathrm{m}}} I_{\mathrm{ionic}}(V_m, n_{dr}, c), \tag{1}$$

$$\frac{dn_{dr}}{dt} = \frac{n_{dr\infty}(V_m) - n_{dr}}{\tau_{n_{dr}}}, \tag{2}$$

$$\frac{dc}{dt} = f\beta(-\alpha(I_{\mathrm{Ca_L}}(V_m) + I_{\mathrm{Ca_T}}(V_m)) - J_{\mathrm{PMCA}}(c))$$

$$+ \frac{1}{v_{cell}}(p_{\mathrm{ER}}(\mathrm{Ca_{ER}}(V_m) - c) - J_{\mathrm{SERCA}}(c)). \tag{3}$$

Model details as well as the values of the parameters used can be found in the Appendix.

System (1)–(3) is an example of a fast-slow system; the variables V_m and n_{dr} change on a considerably faster time scale than c. A standard approach to analysize such systems is to consider the singular limit where the slow variable c is assumed to be constant [13, 20]. In this limit, equations (1) and (2) represent the so-called fast subsystem, which describes the dynamics of the two variables V_m and n_{dr}, and the slow variable c is treated as a parameter.

3   Analysis of the model using the fast subsystem

Both experimental and theoretical results support the claim that BK channels have a large influence on the generation and duration of the active phase of plateau bursting in pituitary cells [3, 4]. Blocking of the BK-channels results in reduction of the BK-type Ca^{2+}-activated K^+ current; see equations (4)–(5) in the Appendix. In our model the fraction of blocked BK channels is expressed by the value of the parameter b_{BK}. We consider both $b_{\mathrm{BK}} = 0$ and $b_{\mathrm{BK}} = 0.15$, that is, the model without any BK channels blocked and with 15% of the open BK channels blocked.

The bursting behavior of the model with $b_{\mathrm{BK}} = 0$ is shown in Fig. 1. Panel (a) shows a time series of both V_m (blue) and c (red) that illustrates pseudo-plateau-bursting oscillations in V_m characterized by an active (bursting) and a silent phase. During the silent phase V_m slowly rises until it reaches a threshold level, which triggers the firing of an action potential (AP). The bursting activity results in an increase of c, because during the active phase there is Ca^{2+} influx through voltage-gated calcium channels. As c reaches a certain concentration, for $b_{\mathrm{BK}} = 0$ it is $c \approx 1~\mu$M, the active phase ends. In the model, this end is caused by the activation of BK channels located further away from the voltage-gated calcium channels ($\mathrm{BK_{FAR}}$; see equation (5) in the Appendix) that repolarize the membrane potential [4] and in this way control the level of $[\mathrm{Ca}^{2+}]_{\mathrm{i}}$. The maximal rise of Ca^{2+} is determined by the number of active BK channels [4, 12]. Note that the duration of the active phase, which in Fig. 1(a) is marked by black dashed lines, is significantly shorter than the duration of the silent phase. Hence, the rise in c is noticeably faster than its decay.

The pseudo-plateau-bursting oscillations in panel (a) correspond to a globally attracting periodic orbit of system (1)–(3). Figure 1(b) shows this periodic orbit, in projection onto the (c, V_m)-plane, as the black closed curve Γ superimposed on the bifurcation diagram of the fast subsys-
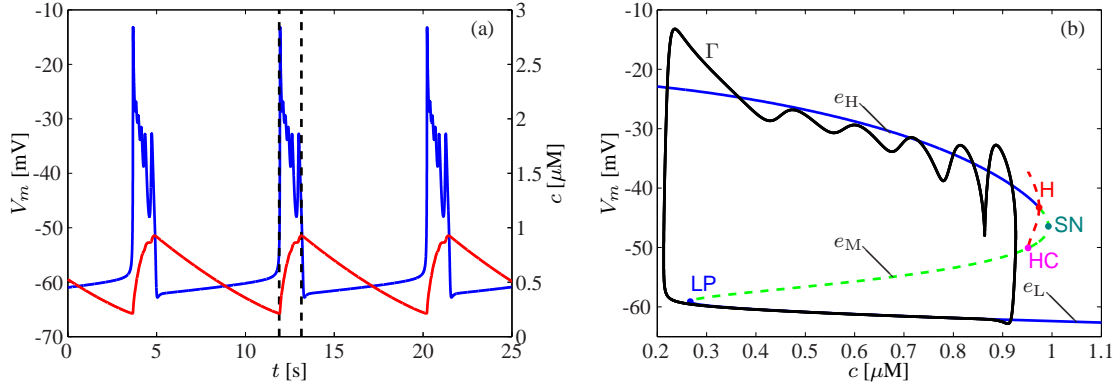
Figure 1: Bursting oscillations in system (1)–(3) with $b_{\mathrm{BK}} = 0$. Panel (a) shows the periodic dynamics of V_m (blue) and c (red) versus time. The active phase is marked by black dashed lines. Panel (b) shows this same periodic orbit Γ (black) overlaid on the bifurcation diagram of the fast subsystem in the (c, V_m)-plane. The solid blue curves are branches of stable equilibria; the dashed green line consists of saddle equilibria; dashed red lines show the maxima and minima of the family of unstable periodic orbits that arises from the Hopf bifurcation point labeled H; this family ends in a homoclinic bifurcation marked HC; labels LP and SN indicate saddle-node bifurcations.

tem (1)–(2). The bifurcation diagram of the fast subsystem (1)–(2) is formed by a Z-shaped branch of equilibria and a family of unstable periodic orbits. The top part of the Z-shaped branch (solid blue curve) is a family e_{H} of stable foci that loses stability at a subcritical Hopf bifurcation marked H; this top part ends at a saddle-node bifurcation labeled SN. The bottom part of the Z-shaped branch is a family e_{L} of stable nodes that also ends at a saddle-node bifurcation, which is labeled LP; the middle branch (dashed green line) in between the two saddle-node bifurcations is a family e_{M} of saddle equilibria. The family of unstable periodic orbits that emanates from the subcritical Hopf bifurcation terminates in a homoclinic bifurcation at e_{M} (labeled HC). In relation to the full system (1)–(3), the branch e_{H} corresponds to the active phase and e_{L} to the silent phase.

The bifurcation diagram of the fast subsystem (1)–(2) is of fold/subHopf type [8] and it is used to explain the behavior of the full system (1)–(3) as follows [13, 20]. The silent phase of Γ occurs along the stable branch e_{L}. Since V_m is low, there is no influx of calcium and c decreases due to efflux. Hence, the phase point tracing Γ approximately follows e_{L} until it reaches LP. The decrease of calcium is accompanied by a gradual increase in the membrane potential, which leads to depolarization that is necessary for the activation of voltage-gated Ca^{2+}-channels. Indeed, the bifurcation diagram of the fast subsystem predicts the thresholds of V_m and c that mediate the transition from the silent to the active phase. As soon as V_m increases beyond the critical value at LP, the active phase begins, which is characterized by a rapid increase of V_m as the phase point of Γ moves up to the only remaining attractor on the branch e_{H}. The rapid change leads to an overshoot followed by several weaker oscillations along e_{H}. Since V_m is high along e_{H}, the voltage-gated Ca^{2+}-channels are open and $[\mathrm{Ca}^{2+}]_{\mathrm{i}}$ starts to increase. Dynamically this means that Γ crosses the c-nullcline and, thus, changes its direction of motion.
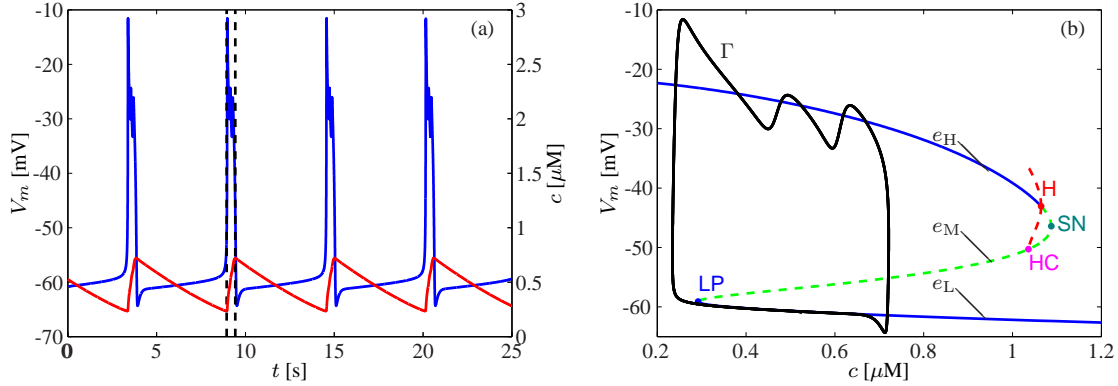
Figure 2: Bursting oscillations in system (1)–(3) with $b_{\mathrm{BK}} = 0.15$. Panel (a) shows the periodic dynamics of V_m (blue) and c (red) versus time. The active phase is marked by black dashed lines. Panel (b) shows this same periodic orbit Γ (black) overlaid on the bifurcation diagram of the fast subsystem in the (c, V_m)-plane. The solid blue curves are branches of stable equilibria; the dashed green line consists of saddle equilibria; dashed red lines show the maxima and minima of the family of unstable periodic orbits that arises from the Hopf bifurcation point labeled H; this family ends in a homoclinic bifurcation marked HC; labels LP and SN indicate saddle-node bifurcations.

Continuing the argument, one expects that the active phase ends at the moment when e_{H} loses stability, that is, at the Hopf bifurcation H, or perhaps at the homoclinic bifurcation HC. However, in contrast to classical plateau-bursting (square-wave or fold/homoclinic) oscillators [6, 8, 21, 22] and pseudo-plateau (fold/subHopf) bursters [7, 9, 10, 11], the oscillations take place away from the family of periodic orbits. Hence, the Hopf and homoclinic bifurcations do not seem to play a role at all in the termination of the active phase of Γ. This same surprising behavior can also be observed for $b_{\mathrm{BK}} = 0.15$ as is shown in Fig. 2. Here, the active phase consists of fewer oscillations, but with larger amplitude. Setting $b_{\mathrm{BK}} = 0.15$ reduces the magnitude of the BK current that is repolarizing in our model, which results in an increase of the rate of change of V_m; see equation (1). As with $b_{\mathrm{BK}} = 0$, the active phase ends long before the Hopf or homoclinic bifurcations. Note that the active phase, labeled by dashed lines in panel (a), is even shorter than for $b_{\mathrm{BK}} = 0$ and ends at a smaller concentration of Ca^{2+}, which only reaches the value of $c \approx 0.7\,\mu\mathrm{M}$. Another major difference between the two cases is the manner in which Γ oscillates during the active phase. For $b_{\mathrm{BK}} = 0$ the oscillations lie mostly below the branch e_{H}, while for $b_{\mathrm{BK}} = 0.15$ the oscillations are always around e_{H}.

The fact that Γ oscillates at all during the active phase requires that the slow variable c changes faster than the speed at which Γ is attracted to e_{H}. In order to establish the rate of convergence, we compute the eigenvalues of the fast subsystem (1)–(2) for each value of V_m along the Z-shaped branch of equilibria. Figure 3 shows the real (top row) and imaginary parts (bottom row) of the eigenvalues for the cases $b_{\mathrm{BK}} = 0$ and $b_{\mathrm{BK}} = 0.15$ in the left and right columns, respectively. Since the eigenvalues of e_{L} are mostly real with rather large negative real parts, there are no oscillations in this region and Γ is sliding along the branch until it reaches LP. Aproximately at LP the orbit Γ jumps to e_{H} and enters the active phase. The family e_{H} are
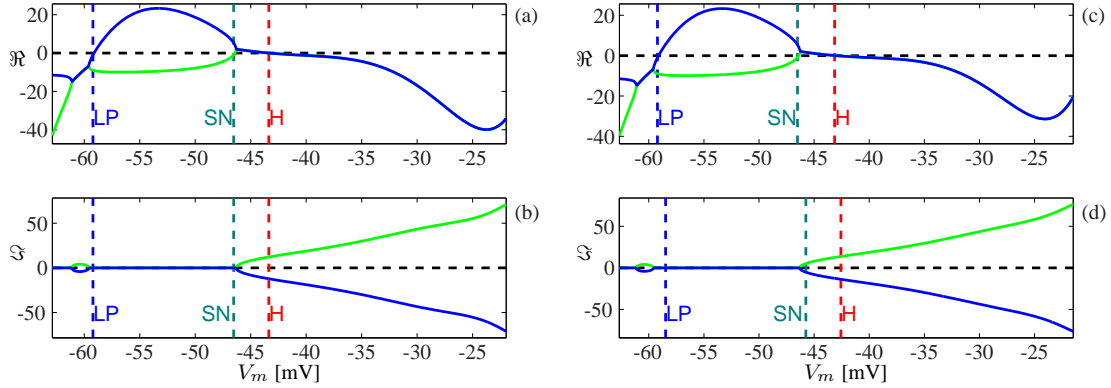
5

Figure 3: Eigenvalues of the fast subsystem with $b_{\mathrm{BK}} = 0$ (left column) and $b_{\mathrm{BK}} = 0.15$ (right column) as a function of V_m along the Z-shaped branch of equilibria e_{L}, e_{M} and e_{H}; panels (a) and (c) show the real parts and panels (b) and (d) the imaginary parts of the eigenvalues; the dotted vertical lines mark the bifurcation points LP, SN and H, respectively.

stable foci and the eigenvalues along this branch are complex conjugate with negative real parts. The transition of Γ from e_{L} to e_{H} is marked by a large overshoot at the beginning of the active phase determined by the magnitude of the eigenvalues at this c value. Fig. 3 shows that the real parts of the eigenvalues along e_{H} are smaller for $b_{\mathrm{BK}} = 0.15$, while the imaginary parts are the same as for $b_{\mathrm{BK}} = 0$. Hence, the rate of convergence is weaker for $b_{\mathrm{BK}} = 0.15$, which causes the difference in amplitudes of the oscillations during the active phase.

4 Oscillations during the active phase

Unfortunately, the analysis of the fast subsystem does not explain why the peaks of the plateau oscillations are below e_{H} for $b_{\mathrm{BK}} = 0$, as illustrated in Fig. 1(b). The oscillations for $b_{\mathrm{BK}} = 0.15$ are clearly around e_{H}, which is more in accordance with the theory [8]; see Fig.2(b). In fact, the theory does not make any statements about this difference in oscillations, but they seem counter-intuitive nonetheless. Let us study the nature of the oscillations in more detail by considering the V_m-nullcline, which separates the regions of increasing and decreasing V_m. We focus on the part of the active phase after the first overshoot.

Figure 4 shows three-dimensional views of one oscillation of Γ (red curve) during the active phase past the overshoot. Panel (a) shows an oscillation for $b_{\mathrm{BK}} = 0$ in the range $c \in [0.519, 0.679]$ μM and panel (b) shows an oscillation for $b_{\mathrm{BK}} = 0.15$ in the range $c \in [0.465, 0.669]$ μM. The V_m-nullcline is a surface in (V_m, n_{dr}, c)-space, shown with a green to yellow gradient, and there are three intersection points with this part of Γ, indicated by red dots. Note that Γ has a local maximum or minum in V_m precisely at these intersection points. The (blue) point cloud is formed by trajectories of the fast subsystem (1)–(2), generated from initial conditions on Γ. As expected, each trajectory converges to the branch e_{H} of stable foci (blue curve). Figure 4 reveals that the oscillatory nature of Γ is essentially the same, except that the second crossing with the V_m-nullcline for $b_{\mathrm{BK}} = 0$ in panel (a) happens below e_{H}, while
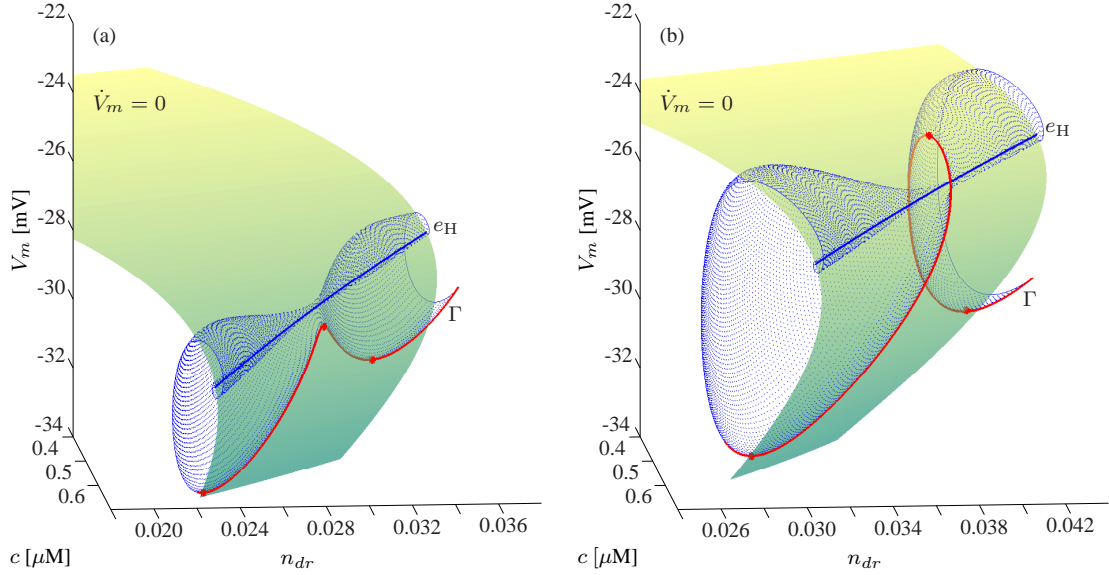
Figure 4: Three-dimensional view of one oscillation of Γ during the active phase for $b_{\mathrm{BK}} = 0$ (a) and $b_{\mathrm{BK}} = 0.15$ (b). The two panels show how Γ (red) interacts with the V_m-nullcline surface (green to yellow gradient). The blue cloud of points are trajectories of the frozen system starting on Γ for different values of c; all these trajectories converge to the family e_{H} (blue curve) on the V_m-nullcline.
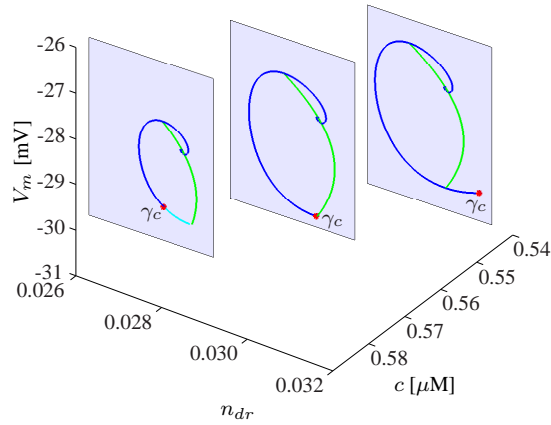

Figure 5: Behavior of trajectories of the fast subsystem with $b_{\mathrm{BK}} = 0$ starting at initial values γ_c (red dots) along the active phase of Γ for $c = 0.541 \ \mu\mathrm{M}$, $c = 0.559 \ \mu\mathrm{M}$ and $c = 0.578 \ \mu\mathrm{M}$, where γ_c lies to the right of, precisely on, and to the left of the V_m-nullcline (green), respectively.

for $b_{\mathrm{BK}} = 0.15$ in panel (b) the second crossing takes place above e_{H}. More precisely, the behavior of Γ is entirely in line with the theory. Let us illustrate this further by considering three cross-sections in the (n_{dr}, V_m)-plane of the phase space shown in Fig.4(a) for $b_{\mathrm{BK}} = 0$, namely, at $c = 0.541 \ \mu\mathrm{M}$, $c = 0.559 \ \mu\mathrm{M}$ and $c = 0.578 \ \mu\mathrm{M}$; see Fig. 5. The trajectories of the fast subsystem generated from initial conditions γ_c on Γ (red dots) are drawn as solid (blue) curves

and the cross-sections illustrate the different behavior depending on the position of the intial condition relative to the V_m-nullcline (green). For $c = 0.541\ \mu$M, the initial condition lies on the right-hand side of the V_m-nullcline and, at first, V_m decreases. Hence the trajectory of the fast subsystem appears to move away from the attractor. For $c = 0.578\ \mu$M the initial condition lies on the left-hand side of the V_m-nullcline and V_m starts to rise immediately. The cross-section at $c = 0.559\ \mu$M illustrates the transition between these two cases, where the trajectory of the fast subsystem starts exactly on the V_m-nullcline. Since Γ has a maximum or minimum precisely at these transition points, the change in the direction of motion satisfies the theory for the fast subsystem, as well as for Γ.

The fact that the oscillations of Γ during the active phase for $b_{\mathrm{BK}} = 0.15$ are able to reach the upper part of the V_m-nullcline surface in Fig. 4(b) means that, in contrast to the case for $b_{\mathrm{BK}} = 0$, the oscillations reach the n_{dr}-nullcline. We illustrate this in Fig. 6(a) by plotting the entire active phase past the first overshoot in $(\dot{V}_m, \dot{n}_{dr}, c)$-space, that is, in terms of the velocities of the fast variables V_m and n_{dr}. The active phase for $b_{\mathrm{BK}} = 0$ (red curve) lasts five oscillations, while the active phase for $b_{\mathrm{BK}} = 0.15$ (cyan curve) is much shorter and lasts only two oscillations after the first overshoot. The horizontal (green) plane at $\dot{V}_m = 0$ is the V_m-nullcline. Note that each oscillation of the active phase both for $b_{\mathrm{BK}} = 0$ and $b_{\mathrm{BK}} = 0.15$ crosses the V_m-nullcline twice. This can most easily be seen in Fig. 6(b), where we plot the projection onto the $(c, \dot{V}_m)$-plane with the V_m-nullcline shown as a dashed (green) line. The vertical (blue) plane at $\dot{n}_{dr} = 0$ is the n_{dr}-nullcline. The active phase for $b_{\mathrm{BK}} = 0.15$ crosses the n_{dr}-nullcline also twice during each revolution. However, for $b_{\mathrm{BK}} = 0$ the first two oscillations do not reach the n_{dr}-nullcline, as is most clearly shown in the projection onto the $(c, \dot{n}_{dr})$-plane in Fig. 6(c). In fact, the third oscillation for $b_{\mathrm{BK}} = 0$ only just crosses the n_{dr}-nullcline; compare also with Fig. 1(b) where the third oscillation after the overshoot barely goes around the branch e_{H}.

Figure 6 indicates that the n_{dr}-nullcline plays an essential role in shaping the oscillations during the active phase. Surprisingly, the n_{dr}-nullcline does not dependend on b_{BK} or c at all. That is, the level of $[\mathrm{Ca}^{2+}]_{\mathrm{i}}$, which is regulated by the value of b_{BK}, does not influence the position of the n_{dr}-nullcline. Hence, the transition happens solely through the variation of Γ. Since the modulation of BK channel activity significantly affects the shape and duration of the active phase it is of interest to obtain an estimate of the critical b_{BK}-value for which the active phase changes from oscillating below to oscillation around e_{H}. We define the moment of this transition as the b_{BK}-value for which the first oscillation of Γ after the initial overshoot is tangent to the n_{dr}-nullcline. This means that $\dot{n}_{dr} = 0$ at the peak of the second oscillation, where $\dot{V}_m = 0$ for the third time. Note that the condition $\dot{n}_{dr} = 0$ as well as $\dot{V}_m = 0$ means that Γ will be tangent to e_{H}. We track the points along the active phase of Γ where $\dot{V}_m = 0$ numerically and continue the third such point in the parameter b_{BK} while monitoring the value of $\dot{n}_{dr}$; the result is shown in Fig. 7. If $\dot{n}_{dr} < 0$ then the first oscillation of Γ after the overshoot will be below e_{H}. If $\dot{n}_{dr} > 0$ then the second peak already lies above e_{H}, so that most likely all oscillations of the active phase are around e_{H}. We determined numerically that the transition happens approximately at $b_{\mathrm{BK}} = 0.07$. The time series of Γ and the associated bifurcation diagram of the fast subsystem for this critical value $b_{\mathrm{BK}} = 0.07$ are shown in Fig. 8; compare also with Figs. 1 and 2.
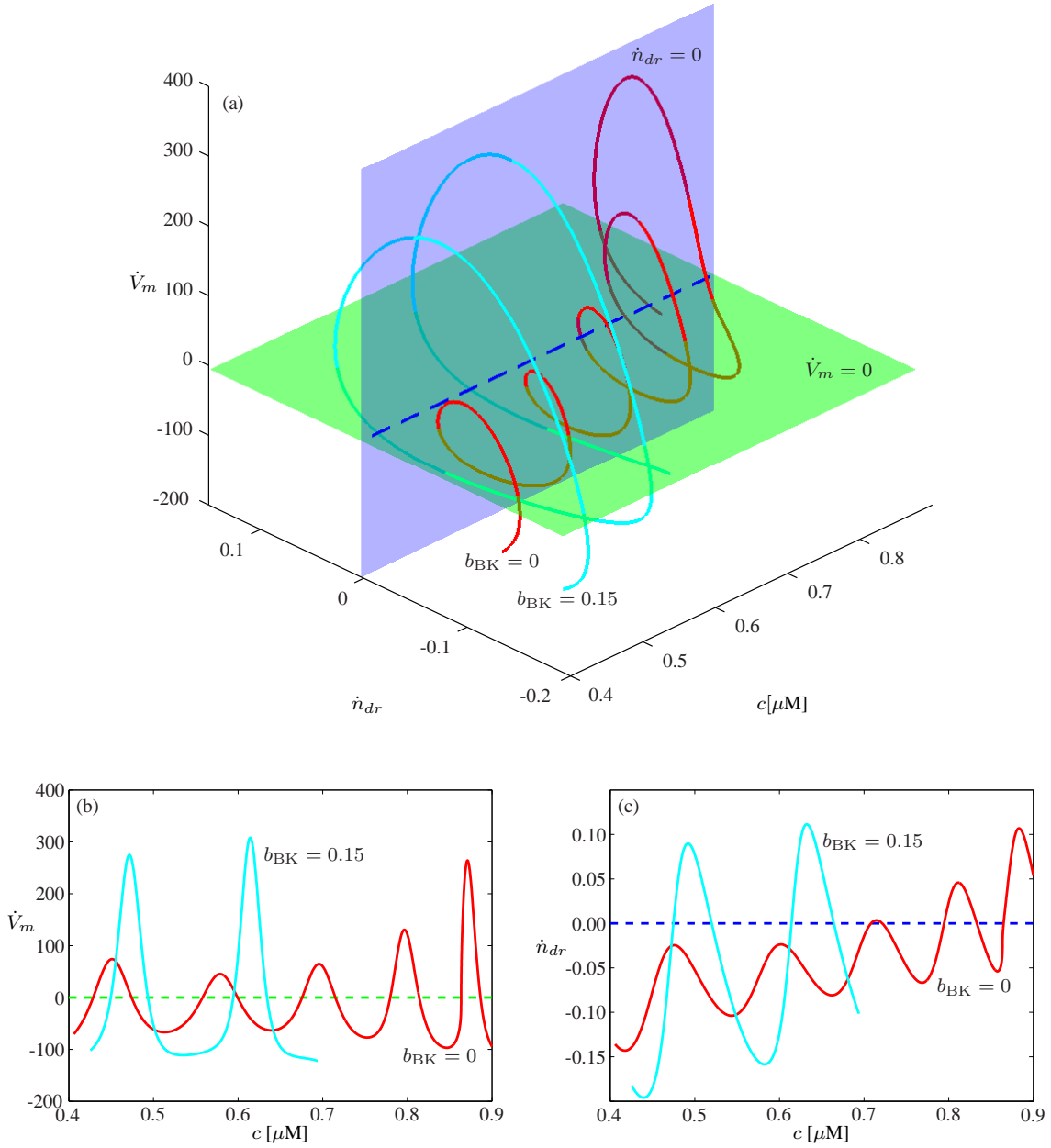
Figure 6: The active phase of Γ past the first overshoot for $b_{\mathrm{BK}} = 0$ (red curve) and $b_{\mathrm{BK}} = 0.15$ (cyan curve) plotted in $(\dot{V}_m, \dot{n}_{dr}, c)$-space (a) along with projections onto the $(c, \dot{V}_m)$- and $(c, \dot{n}_{dr})$-planes in panels (b) and (c), respectively. The nullclines $\dot{V}_m = 0$ (green horizontal plane) and $\dot{n}_{dr} = 0$ (blue vertical plane) in panel (a) project to the dashed lines in panels (b) and (c), respectively.
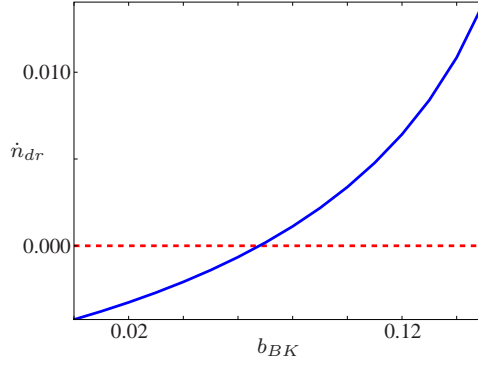
Figure 7: The value of $\dot{n}_{dr}$ at the peak of the second oscillation in the active phase of Γ as a function of $b_{\mathrm{BK}} \in [0, 0.15]$. The crossing at $\dot{n}_{dr} = 0$ marks the transition from oscillations below e_{H} to oscillations around e_{H} in system (1)–(3).
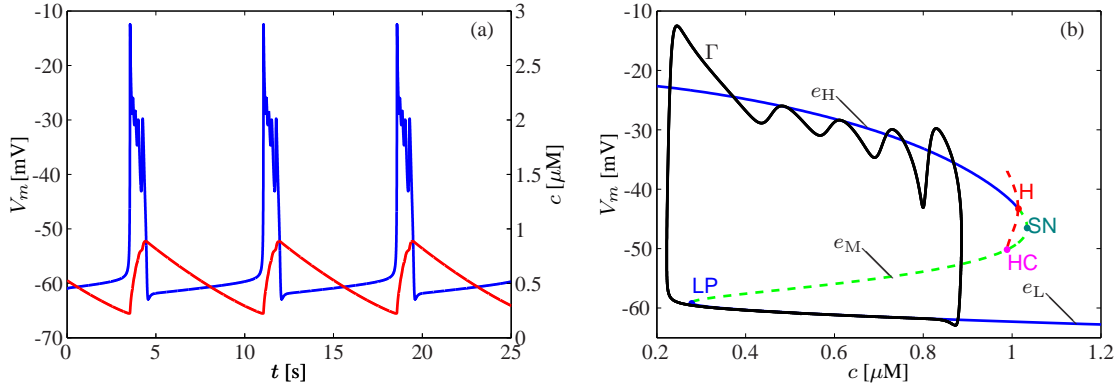

Figure 8: Bursting oscillations in system (1)–(3) with $b_{\mathrm{BK}} = 0.07$. Panel (a) shows the periodic dynamics of V_m (blue) and c (red) versus time. Panel (b) shows this same periodic orbit Γ (black) overlaid on the bifurcation diagram of the fast subsystem in the (c, V_m)-plane. The solid blue curves are branches of stable equilibria; the dashed green line consists of saddle equilibria; dashed red lines show the maxima and minima of the family of unstable periodic orbits that arises from the Hopf bifurcation point labeled H; this family ends in a homoclinic bifurcation marked HC; labels LP and SN indicate saddle-node bifurcations.

5   The end of the active phase

Modulating the BK current not only affects the position of the oscillations in the active phase relative to the equilibrium branch e_{H}. Figures 1, 2, and 8 show that increasing b_{BK} dramatically alters the duration of the active phase. The active phase contains six oscillations for $b_{\mathrm{BK}} = 0$ and ends relatively close to the homoclinic bifurcation HC, but for $b_{\mathrm{BK}} = 0.07$ there are five oscillations, and for $b_{\mathrm{BK}} = 0.15$ only three oscillations remain, while the end of the active phase moves increasingly further away to the left of HC. Note that the variation of b_{BK} has almost no effect on the bifurcation diagram of the fast subsystem, so that this cannot be the mechanism behind the termination of the active phase.
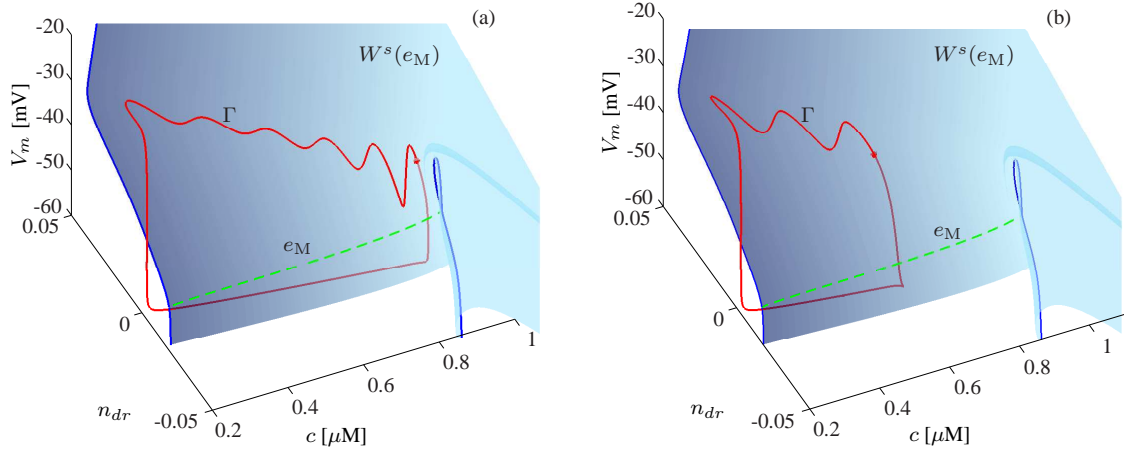
Figure 9: The c-dependent family $W^s(e_M)$ of one-dimensional stable manifolds of the saddle points along e_M in between LP and HC. Panel (a) shows the manifold for $b_{BK} = 0$ and panel (b) for $b_{BK} = 0.15$ along with the family e_M of saddle equilibria (green dashed line). The manifold $W^s(e_M)$ is shown as a blue gradient surface with two solid (blue) lines marking the bounding manifolds at LP and HC. The orbit Γ is depicted as a solid (red) curve.

Since we have coexisting attractors for the range of c that corresponds to the active phase, the end of the active phase must be explained by the fact that Γ leaves the basin of attraction of e_H, thereby entering the basin of attraction of e_L. The projection onto the (c, V_m)-plane of the bifurcation diagram of the fast subsystem appears to indicate that the branch e_M of saddle equilibria separates the two basins of attraction. However, in the full (V_m, n_{dr}, c)-space the separatrix is formed by the family of one-dimensional stable manifolds of the saddle points on e_M. This family, denoted $W^s(e_M)$, is a well-defined manifold for saddle points on e_M in between the saddld-node bifurcation LP and the homoclinic bifurcation HC; note that the family of one-dimensional stable manifolds continues to exist for points on e_M past HC, but then the manifols are no longer separating the basins of attraction.

We compute the family $W^s(e_M)$ via continuation of a one-parameter family of two-point boundary value problems [23]. The manifold $W^s(e_M)$ is parametrized by c and the computation effectively generates a family of orbit segments that start at a point on the (c-dependent) stable eigenvector sufficiently close to the (c-dependent) saddle point on e_M; we refer to [23, 24] for details on the precise boundary conditions. The branches starting along the eigendirection with positive V_m were computed up to arclength 60 and those with negative V_m up to arclength 10. Figure 9 shows $W^s(e_M)$ as a blue gradient surface with the associated equilibria on e_M marked by a dashed (green) line. Panel (a) shows the manifold for $b_{BK} = 0$ and panel (b) for $b_{BK} = 0.15$. In both cases the corresponding orbit Γ is shown as well (red curve).

The manifolds $W^s(e_M)$ for $b_{BK} = 0$ and $b_{BK} = 0.15$ are quite similar. For low values of c the surface is relatively straightforward with each one-dimensional manifold having one side (the upper branch) extend toward $-\infty$ and the other side extend toward $+\infty$ for both V_m and n_{dr}. The first bounding manifold on this side is shown as a thick (blue) curve and corresponds to the manifold at the moment of the saddle-node bifurcation (LP). The manifolds vary smoothly

11

with c and, in fact, they hardly change initially as c increases. The other side of $W^s(e_M)$ is bounded by the homoclinic bifurcation, which is again shown as a thick (blue) curve. Here, the one-dimensional stable manifold of the corresponding saddle equilibrium on e_M must have its upper branch fold over and connect back to this saddle equilibrium. Since the family of manifolds depends smoothly on c, one expects to see the folding happening slightly earlier, for slightly smaller values of c, so that the upper branch comes back below the corresponding saddle equilibrium and folds exponentially flat onto the lower branch, also extending to $-\infty$ for both V_m and n_{dr}. The start of this process can be observed in Fig. 9 as the darker shaded band running through the lighter side of $W^s(e_M)$, which is caused by the smaller steps taken in the continuation to capture the dramatic change of the one-dimensional manifolds here.

While the expected folding of the manifolds does take place before the homoclinic bifurcation, it happens only for a relatively small range of c-values and there is little difference between the manifolds for $b_{BK} = 0$ and $b_{BK} = 0.15$. This means that b_{BK} has no noticeable influence on the shape of the basin of attraction of e_H. Hence, similar to what was the case for the oscillations below or around e_H, the parameter b_{BK} only influences the shape of the orbit Γ itself such that its position with respect to $W^s(e_M)$ changes. Indeed, b_{BK} has the effect of increasing the amplitude of the oscilations of Γ during the active phase. This increase causes Γ to lie closer to $W^s(e_M)$ so that is crosses $W^s(e_M)$ for increasingly smaller values of c. As illustrated in Fig. 9, as soon as Γ crosses $W^s(e_M)$, it drops down to e_L and the active phase ends.

Therefore, the behavior of system (1)–(3) can be explained using the fast subsystem (1)–(2), but the bifurcation analysis must include the computation of the stable manifolds that bound the basins of attraction of e_H and e_L that represent the active and silent phases, respectively. As we already noted earlier, the fast subsystem is, however, not noticeably affected when a fraction of the BK channels is blocked. The parameter b_{BK} only influences the amplitude of Γ, which may be inferred from inspecting the contraction rates along the branch e_H, but is extremely subtle. An increase in amplitude causes Γ to oscillate closer to $W^s(e_M)$ already for small values of c, which leads to the earlier termination of the active phase.

6   Conclusion

We performed a detailed analysis of a fast-slow single-compartment physiologically-based cell model of fold/subHopf type. We used a reduced version of a somatotroph cell model by Tsaneva-Atanasova et al. [4] that includes modulation of the BK channels, controlled by the parameter b_{BK}. As previously reported in [3, 4], blocking of the BK channels significantly influences the model behavior. We considered the cases of no ($b_{BK} = 0$) and 15% blocking ($b_{BK} = 0.15$). In order to understand fully the behavior of the bursting trajectories in our model we had to consider dynamical systems techniques other than the classical bifurcation analysis of the corresponding fast subsystem, where one considers the singular limit of stationary slow flow. We analyzed the seemingly counterintuitive behavior of the plateau bursting taking place below the branch of attracting equilibria of the fast subsystem that corresponds to the active phase. Furthermore, we used continuation to compute the basin boundary of this branch of attracting equilibria of the fast subsystem as a family of one-dimensional stable manifolds of saddle equilibria. Our

computation showed that this surface marks the end of the active phase.

Despite the fact that our model exhibits a well-known fold/subHopf bifurcation structure for the fast subsystem, the pseudo-plateau-bursting behavior is subtly different from that found in other fold/subHopf bursting model systems [7, 9, 10, 11] and clearly different from the behavior of classical square-wave (fold/Homoclinic) bursters [6, 8, 21, 22]. Most importantly, blocking of BK channels does not significantly alter the underlying bifurcation diagram of the fast subsystem, including the family of stable manifolds. However, it has a profound effect on the shape and duration of the bursting oscillations during the active phase.

Given the importance of the rapid ionic activities in pituitary cells that set the levels of $[Ca^{2+}]_i$ [3, 4] and are instrumental for the regulation of hormone exocytosis [1, 2], it is important to identify key determinants of these activities. This is not merely of academic interest, as it may have implications for the hormone release process via modulation of the intracellular calcium levels. Indeed, changing the conductance of voltage-gated K^+ channels or K_{Ca} channels, such as the BK channel, changes the spike amplitude in the active phase of a burst as well as its duration. This voltage sensitivity consequently results in a decreased level of $[Ca^{2+}]_i$ that is ultimately associated with reduced hormonal secretion [1]. Some effects of BK blockade and natural variation of BK channel density were discussed in [4], and BK blockade was shown to convert apparent pseudo-plateau bursting in pituitary somatotrophs to large-amplitude spiking [3]. Similar effects are seen by varying the time constant of voltage-gated K^+ channels or the conductance of voltage-dependent Ca^{2+} channels (unpublished observations). Although the emphasis here has been on the dynamical structures of the model, our results with regard to the effect that blocking of the BK channels has on the shape and duration of the bursting active phase oscillations could be interpreted in a broader context. They imply that any modification in the currents underlying pseudo-plateau bursting that leads to the increase in the rate of change of the fast variables should result in shorter burst duration, provided that the bifurcation diagram of the fast subsystem remains almost unchanged.

The general understanding of the mechanism involved in control of the behavior of secretory anterior pituitary cells is very important, because these cells play a major role in the homeostasis. Organized by the hypothalamus, the pituitary cells are releasing vital hormones. We focused our interest on pituitary somatotrophs, which fire plateau-burst APs to generate Ca^{2+} signals to trigger the secretion of growth hormone. However, our analysis and techniques are also applicable to other models of pituitary cells and broaden the tools for investigating their dynamics.

Acknowledgments

References

[1] F. van Goor, D. Zivadinovic, A. J. Martinez-Fuentes, S. S. Stojilkovic, Dependence of pituitary hormone secretion on the pattern of spontaneus voltage-gated calcium influx: cell-type specific action potential-secretion coupling, Journal of Biological Chemistry 276 (36) (2001) 33840–33846.

[2] S. S. Stojilkovic, H. Zemkova, F. van Goor, Biophysical basis of pituitary cell type-specific Ca^{2+} signaling-secretion coupling, Trends in Endocrinology and Metabolism 16 (4) (2005) 152–159.

[3] F. van Goor, Y. X. Li, S. S. Stojilkovic, Paradoxical role of large-conductance calcium-activated K^+ (BK) channels in controlling action potential-driven Ca^{2+} entry in anterior pituitary cells, Journal of Neuroscience 21 (16) (2001) 5902–15.

[4] K. Tsaneva-Atanasova, A. Sherman, F. van Goor, S. S. Stojilkovic, Mechanism of spontaneous and receptor-controlled electrical activity in pituitary somatotrophs: Experiments and theory, Journal of Neurophysiology 98 (1) (2007) 131–144.

[5] A. L. Hodgkin, A. F. Huxley, A quantitative description of membrane current and its application to conduction and excitation in nerve, Journal of Physiology 117 (4) (1952) 500–544.

[6] J. Keener, J. Sneyd, Mathematical Physiology, 2nd Edition, Springer-Verlag, New York, 2009.

[7] J. Stern, H. M. Osinga, A. LeBeau, A. Sherman, Resetting behavior in a model of bursting in secretory pituitary cells: Distinguishing plateaus from pseudo-plateaus, Bulletin of Mathematical Biology 70 (1) (2008) 68–88.

[8] E. M. Izhikevich, Neural excitability, spiking, and bursting, International Journal of Bifurcation and Chaos 10 (6) (2000) 1171–1266.

[9] A. P. LeBeau, A. B. Robson, A. E. McKinnon, J. Sneyd, Analysis of a reduced model of cortiocotroph action potentials, Journal of Theoretical Biology 192 (3) (1998) 319–339.

[10] J. Tabak, N. Toporikova, M. Freeman, R. Bertram, Low dose of dopamine may stimulate prolactin secretion by increasing fast potassium currents, Journal of Computational Neuroscience 22 (2) (2007) 211–22.

[11] N. Toporikova, J. Tabak, M. Freeman, R. Bertram, A-type K^+ current can act as a trigger for bursting in the absence of a slow variable, Neural Computation 20 (2) (2008) 436–51.

[12] B. Fakler, J. P. Adelman, Control of K_{Ca} channels by calcium nano/microdomains, Neuron 59 (6) (2008) 873–881.

[13] J. Rinzel, Bursting oscillations in an excitable membrane model, in B. D. Sleeman, R. J. Jarvis (Eds.), Ordinary and Partial Differential Equations, Lecture Notes in Mathematics Vol. 1151, Springer-Verlag, New York (1985), pp. 304–316.

[14] Yu. A. Kuznetsov, Elements of Applied Bifurcation Theory, Springer-Verlag, New York, 1998.

[15] S. H. Strogatz, Nonlinear Dynamics and Chaos: With Applications to Physics, Biology, Chemistry and Engineering, Perseus Books, 2001.

[16] E. J. Doedel, AUTO, a program for the automatic bifurcation analysis of autonomous systems, Congressus Numerantium 30 (1981) 265–384.

[17] E. J. Doedel, R. C. Paffenroth, A. R. Champneys, T. F. Fairgrieve, Yu. A. Kuznetsov, B. E. Oldeman, B. Sandstede, and X. J. Wang, AUTO-07P: Continuation and bifurcation software for ordinary differential equations (2007); available via http://cmvl.cs.concordia.ca/.

[18] B. Ermentrout, Simulating, Analyzing, and Animating Dynamical Systems: A Guide To Xppaut for Researchers and Students, Society for Industrial and Applied Mathematics, Philadelphia, 2002.

[19] MATLAB, The MathWorks Inc., Natick, MA (2008); http://www.mathworks.com

[20] N. Fenichel, Persistence and smoothness of invariant manifolds for flows, Indiana University Mathematics Journal 21 (1972) 193–226.

[21] R. Bertram, M. Butte, T. Kiemel, A. Sherman, Topological and phenomenological classification of bursting oscillations, Bulletin of Mathematical Biology 57 (3) (1995) 413–439.

[22] A. L. Shilnikov, M. Kolomiets, Methods of the qualitative theory for the Hindmarsh-Rose model: a case study. Tutorial, International Journal of Bifurcation and Chaos 18 (8) (2008) 2141–2168.

[23] B. Krauskopf, H. M. Osinga, Computing invariant manifolds via the continuation of orbit segments, in B. Krauskopf, H. M. Osinga and J. Galán-Vioque (Eds.), Numerical Continuation Methods for Dynamical Systems: Path following and boundary value problems, Springer-Verlag, New York (2007), pp. 117–154.

[24] B. Krauskopf, T. Rieß, A Lin's method approach to finding and continuing heteroclinic connections involving periodic orbits, Nonlinearity 21(8) (2008) 1655–1690.

Appendix

In this appendix we provide the complete details of our model (1)–(3). The functional dependencies are discussed in order below and the values of the parameters used for the model are given in Table 1.

Equation (1) is a capacitance model of V_m, where C_m stands for the membrane capacitance and I_{ionic} is the sum of ionic currents

$$
\begin{aligned}
I_{\text{ionic}} &= I_{\text{Ca}_L}(V_m) + I_{\text{Ca}_T}(V_m) + I_{\text{K}_{dr}}(V_m, n_{dr}) + I_{\text{K}_{ir}}(V_m) \\
&\quad + I_{\text{NS,Na}}(V_m) + I_{\text{BK}_{\text{NEAR}}}(V_m) + I_{\text{BK}_{\text{FAR}}}(V_m, c).
\end{aligned}
$$

Here, I_{Ca_L} and I_{Ca_T} are L- and T-type voltage-sensitive Ca^{2+}-currents of the form

$$
\begin{aligned}
I_{\text{Ca}_L}(V_m) &= g_{\text{Ca}_L} m^2_{\text{Ca}_{L\infty}}(V_m)(V_m - V_{\text{Ca}}), \\
I_{\text{Ca}_T}(V_m) &= g_{\text{Ca}_T} m^2_{\text{Ca}_{T\infty}}(V_m) h_{\text{Ca}_{T\infty}}(V_m)(V_m - V_{\text{Ca}}).
\end{aligned}
$$

The corresponding activation and inactivation functions are given by

$$
m_{\text{Ca}_{L\infty}}(V_m) = \frac{1}{1 + \exp\left(\frac{-(V_m - V_{\text{m}_L})}{k_{\text{m}_L}}\right)},
$$

$$
m_{\text{Ca}_{T\infty}}(V_m) = \frac{1}{1 + \exp\left(\frac{-(V_m - V_{\text{m}_T})}{k_{\text{m}_T}}\right)} \quad \text{and}
$$

$$
h_{\text{Ca}_{T\infty}}(V_m) = \frac{1}{1 + \exp\left(\frac{V_m - V_{\text{h}_T}}{k_{\text{h}_T}}\right)}.
$$

The currents $I_{\text{K}_{dr}}$ and $I_{\text{K}_{ir}}$ are delayed-rectifier and inward-rectifier of K^+-currents, expressed as

$$
\begin{aligned}
I_{\text{K}_{dr}}(V_m, n_{dr}) &= g_{\text{K}_{dr}} n_{dr}(V_m - V_{\text{K}}) \quad \text{and} \\
I_{\text{K}_{ir}}(V_m) &= g_{\text{K}_{ir}} \text{K}_{ir\infty}(V_m)(V_m - V_{\text{K}_{ir}}).
\end{aligned}
$$

The rate of change of the fraction of open delay-rectifier K^+-channels n_{dr} follows the dynamics given by equation (2), with the steady-state function defined as

$$
n_{dr\infty}(V_m) = \frac{1}{1 + \exp\left(\frac{-(V_m - V_{n_{dr}})}{k_{n_{dr}}}\right)}.
$$

The steady-state function for $I_{\text{K}_{ir}}$ is given by

$$
\text{K}_{ir\infty}(V_m) = \frac{\alpha_{\text{ir}}}{\alpha_{\text{ir}} + \beta_{\text{ir}}},
$$

where

$$
\begin{aligned}
\alpha_{\text{ir}}(V_m) &= \frac{0.1}{1 + \exp[0.06(V_m - V_{\text{K}_{ir}} - 200)]}, \\
\beta_{\text{ir}}(V_m) &= \frac{3\exp[0.0002(V_m - V_{K_{ir}} + 100)] + \exp[0.1(V_m - V_{K_{ir}} - 10)]}{1 + \exp[-0.5(V_m - V_{\text{K}_{ir}})]}.
\end{aligned}
$$

Table 1: Parameter values used in the simulations.

Parameter	Value		Parameter	Value	
$g_{\mathrm{Ca_L}}$	0.74	nS	$k_{\mathrm{m_T}}$	8	mV
$g_{\mathrm{Ca_T}}$	0.105	nS	$V_{\mathrm{h_T}}$	-56	mV
$g_{\mathrm{K_{dr}}}$	3.85	nS	$k_{\mathrm{h_T}}$	5	mV
$g_{\mathrm{K_{ir}}}$	15.75	nS	$V_{n_{dr}}$	0	mV
$g_{\mathrm{BK_{NEAR}}}$	0.55	nS	$k_{n_{dr}}$	8	mV
$g_{\mathrm{BK_{FAR}}}$	10	nS	k_{BK}	10	mV
$g_{\mathrm{NS,Na}}$	0.1245	nS	$V_{\mathrm{BK_0}}$	0.1	mV
V_{Ca}	60	mV	k_{shift}	18	
V_{K}	-80	mV	$k_{\mathrm{Ca_{bk}}}$	1.5	μM
$V_{\mathrm{K_{ir}}}$	-83	mV	A	0.11	
$V_{\mathrm{NS,Na}}$	-20	mV	f	0.0098	
σ_{N}	0.002	pA	p_{ER}	0.00015	s^{-1}
$\tau_{n_{dr}}$	0.09	s	d_{cell}	10	μm
$V_{\mathrm{m_L}}$	-25	mV	V_{PMCA}	28	μM.s^{-1}
$k_{\mathrm{m_L}}$	12	mV	K_{PMCA}	0.08	μM
$V_{\mathrm{m_T}}$	-45	mV	k_{SERCA}	0.025	μM.s^{-1}
C_{m}	0.00314	mF	$\mathrm{Ca_{ER}}$	167	μM

The currents of the BK channels $I_{\mathrm{BK_{NEAR}}}$ and $I_{\mathrm{BK_{FAR}}}$ are located near and far from voltage-gated Ca^{2+}-channels; they are given by

$$I_{\mathrm{BK_{NEAR}}}(V_m) = (1 - b_{\mathrm{BK}})g_{\mathrm{BK_{NEAR}}}b_{\mathrm{K_{NEAR}\infty}}(V_m)(V_m - V_K) \text{ and} \tag{4}$$

$$I_{\mathrm{BK_{FAR}}}(V_m, c) = (1 - b_{\mathrm{BK}})g_{\mathrm{BK_{FAR}}}b_{\mathrm{K_{FAR}\infty}}(V_m, c)(V_m - V_K). \tag{5}$$

The parameter b_{BK} expresses the fraction of blocked BK channels. The steady-state functions for these currents are

$$b_{\mathrm{K_{NEAR}\infty}}(V_m) = \frac{1}{1 + \exp\left(\frac{-(V_m - V_{\mathrm{BK_{NEAR}}}(V_m))}{k_{\mathrm{BK}}}\right)} \text{ and}$$

$$b_{\mathrm{K_{FAR}\infty}}(V_m, c) = \frac{1}{1 + \exp\left(\frac{-(V_m - V_{\mathrm{BK_{FAR}}}(c))}{k_{\mathrm{BK}}}\right)},$$

where

$$V_{\mathrm{BK_{NEAR}}}(V_m) = V_{\mathrm{BK_0}} - k_{\mathrm{shift}} \ln \frac{Ca_{\mathrm{DOM}}(V_m)}{k_{\mathrm{Ca_{BK}}}},$$

$$V_{\mathrm{BK_{FAR}}}(c) = V_{\mathrm{BK_0}} - k_{\mathrm{shift}} \ln \frac{c}{k_{\mathrm{Ca_{BK}}}} \text{ and}$$

$$Ca_{\mathrm{DOM}}(V_m) = -A(I_{\mathrm{Ca_L}}(V_m) + I_{\mathrm{Ca_T}}(V_m)).$$

Finally, $I_{\mathrm{NS,Na}}$ is a non-selective predominantly Na^+-current, given by

$$I_{\mathrm{NS,Na}}(V_m) = g_{\mathrm{NS,Na}}(V_m - V_{\mathrm{NS,Na}}).$$

The parameter β in equation (3) is the ratio of cell surface area A_{cell} and volume V_{cell}, expressed by

$$A_{\mathrm{cell}} = \pi d_{\mathrm{cell}}^2 \text{ and } v_{\mathrm{cell}} = \frac{\pi d_{\mathrm{cell}}^3}{6},$$

where d_{cell} is the diameter of the cell. The parameter α converts the calcium currents in (3) into fluxes and is given by

$$\alpha = \frac{1}{2 F A_{\mathrm{cell}}},$$

where F is Faraday's constant. The individual Ca^{2+}-fluxes due to the Ca^{2+}-ATP-pumps of the plasma membrane and endoplasmic reticulum (ER) are

$$J_{\mathrm{PMCA}}(c) = V_{\mathrm{PMCA}} \frac{c^2}{c^2 + K_{\mathrm{PMCA}}^2} \text{ and } J_{\mathrm{SERCA}}(c) = k_{\mathrm{SERCA}} c.$$